

# Topological band and superconductivity in $\text{UTe}_2$

Tatsuya Shishidou,<sup>1</sup> Han Gyeol Suh,<sup>1</sup> P. M. R. Brydon,<sup>2</sup> Michael Weinert,<sup>1</sup> and Daniel F. Agterberg<sup>1</sup>

<sup>1</sup>*Department of Physics, University of Wisconsin, Milwaukee, WI 53201, USA*

<sup>2</sup>*Department of Physics and MacDiarmid Institute for Advanced Materials and Nanotechnology, University of Otago, P.O. Box 56, Dunedin 9054, New Zealand*

$\text{UTe}_2$  has recently been found to be a likely spin-triplet superconductor that exhibits evidence for chiral Majorana edge states. A characteristic structural feature of  $\text{UTe}_2$  is inversion-symmetry related pairs of U atoms, forming rungs of ladders. Here we show how each rung's two sublattice degrees of freedom play a key role in understanding the electronic structure and the origin of superconductivity. In particular, we show that DFT+ $U$  calculations generically reveal a topological band that originates from a band inversion associated with  $5f$  electrons residing on these rung sublattice degrees of freedom. Furthermore, we show that a previously identified strong ferromagnetic interaction within a U-U rung leads to a pseudospin-triplet superconducting state that can account for a non-zero polar Kerr angle, observed magnetic field-temperature phase diagrams, and nodal Weyl fermions. Our analysis may also be relevant for other U-based superconductors.

$\text{UTe}_2$  [1] is poised to become a paradigmatic superconductor exhibiting unconventional behavior: Superconductivity survives to much higher magnetic fields than expected [1–9] and shows a highly unusual re-entrant field induced superconductivity [10]. Furthermore, there is evidence for ferromagnetic fluctuations [11, 12], odd-parity superconductivity [13], multiple superconducting phases [14–18], spontaneous broken time-reversal symmetry [15], and chiral Majorana edge and surface states [19, 20], the nature of which are not yet understood.

Many important questions remain open in understanding this material, foremost of which is the origin of the odd-parity superconductivity. There is a consensus that ferromagnetic fluctuations are responsible for the pairing in the related  $\text{UGe}_2$ ,  $\text{URhGe}$ , and  $\text{UCoGe}$  compounds, [21], but uncertainty as to the appropriate underlying model has led to debate over the nature of these ferromagnetic fluctuations [21]. Recently, this question has been addressed in  $\text{UTe}_2$  [22–24] where density functional theory plus Hubbard  $U$  (DFT+ $U$ ) and dynamical mean field theory (DMFT) calculations have developed a family of band structures that depend upon  $U$ . The consequences of this family of band structures on superconductivity have been explored, suggesting topological superconductivity [24]. In addition, effective Heisenberg theories have been developed, with the insight that the strongest magnetic interaction, for all  $U$  values considered, is a ferromagnetic interaction between the two nearest-neighbor U atoms on a ladder rung [23], providing a potential mechanism for superconductivity.

Here we revisit the DFT+ $U$  calculations, finding good agreement with previous results and newly identifying a topological band that appears near the chemical potential for all values of  $U$ . This topological band has its origin in the  $5f$  electrons located predominantly on the rung sublattice degrees of freedom. On the two U atoms of the rung, a band inversion between even- and odd-parity orbital combinations provides the origin of the topological band. The appearance of the topological band together

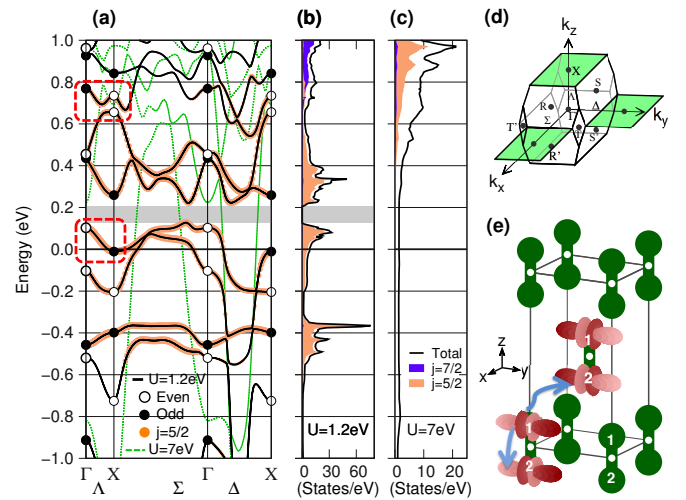


FIG. 1. (a) Two DFT+ $U$  bands:  $U=1.2$  eV (black solid lines) and 7 eV (green line) where  $5f$  electrons do and do not participate in the Fermi surface formation, respectively. For the former, the even/odd band parity and  $j=5/2$  component are shown by the open/closed circles (black) and fat band representation (orange), respectively. The grey shaded region lying above the energy zero (chemical potential) represents a 81 meV bandgap that separates a pair of topological  $5f$  bands, indicated by red-dotted boxes along the  $\Lambda$  direction. Density of states for (b)  $U=1.2$  eV and (c) 7 eV. (d) First BZ and eight TRIMs. Additional X faces (green) of the neighboring BZs are shown to demonstrate that all three principal  $k$  lines ( $\Lambda$ ,  $\Sigma$ , and  $\Delta$ ) connect  $\Gamma$  and X. (e) Wave function schematics of topological band at X point with odd parity. Thin/thick shading of lobes represents their positive/negative sign. In accord with the wave vector  $k=(0,0,2\pi)$ , the sign array of body-centered orbitals is reversed from that of corner-centered.

with the rung ferromagnetic interaction discussed above indicates that the rung sublattice degrees of freedom play a central role in the electronic description. Consequently, we construct a symmetry-based electronic model that explicitly includes these rung sublattice degrees of freedom and the ferromagnetic interaction between them. This

model yields magnetic field-temperature phase diagrams that agree with experiment, allows a superconducting state with Weyl nodes, and provides an explanation for the observed surface chiral edge states [20], the observed polar Kerr effect [15], and observed low energy excitations in the superconducting state [25].

*Topological Band:* A likely scenario for the electronic structure of UTe<sub>2</sub> is a low temperature renormalized Fermi liquid ground state in which U 5*f* electrons are participants. This is consistent with scanning tunneling microscopy [20] and the observed Fermi pocket about the *X*-point seen in ARPES data [26, 27] (called *Z* in Ref. 27). This point of view has been adopted in recent DMFT and DFT+*U* calculations [22–24]. The latter reveals that the band structure depends strongly on the choice of *U*, suggesting that any theory of the superconducting state needs to be developed for a range of band structures, emphasizing properties that are generic across the relevant possibilities. Here, we have carried out DFT calculations of the band structure of UTe<sub>2</sub> using the full-potential linearized augmented plane wave method [28] and including a Coulomb *U* to account for interactions of the U 5*f* electrons. Our results agree with those found earlier [23, 24]. A key new finding is that for all values of *U* included here, we find a topological band at or near the chemical potential.

As reported earlier, the band structure differs significantly along the three principal *k* axes due to the underlying quasi one-dimensional (1D) bands, whose features vividly unfold in the no 5*f* electron limit or, equivalently, in the large *U* limit as shown in Fig. 1(a). The quasi-1D bands arise from the U 6*d* dimer state which strongly disperses along the *k<sub>x</sub>* ( $\Sigma$ ) direction, and also the Te 5*p* linear chain state which disperses along the *k<sub>y</sub>* ( $\Delta$ ) direction. For realistic values of *U* (see the *U* = 1.2eV band in Fig. 1(a)), the 5*f* states are able to hybridize with these bands, leading to rather complicated dispersions along  $\Sigma$  and  $\Delta$ . In contrast, the 5*f* dispersion along  $\Lambda$  is much simpler and we can make the following observations for the *j* = 5/2 sector: (i) Among the six Kramers-degenerate bands, two are *topologically nontrivial* in the sense that the band parity switches between  $\Gamma$  and *X*, while the other four bands do not show such parity change; (ii) these two are well separated in energy; (iii) the lower energy band, located near the chemical potential (energy zero), has even parity at  $\Gamma$  and odd at *X*; and (iv) of the four trivial bands, a set of odd- and even-parity bands are occupied.

These features persistently exist regardless of *U*. The band structure and density of states (DOS) plots [Fig. 1(b)(c)], however, constrain the range of *U* that reproduce the experimental results such as strong ARPES signals around  $-0.5$  eV [26] or  $-0.7$  eV [27]. In particular, for a range of moderate *U* ( $1.1$  eV  $\leq U \leq 2.0$  eV), a band gap appears just above the lower nontrivial band; the Hilbert space below this gap (corresponding to the

occupied levels of a +2*e* doped system) is characterized by  $Z_2$  topological invariants ( $\nu_0; \nu_1, \nu_2, \nu_3$ ) [29], which are found from the knowledge of band parity at eight time-reversal-invariant momenta (TRIMs). Due to a mirror symmetry duplication of *R*, *S*, and *T* [c.f., Fig. 1(d)], the index  $\nu_0$  is determined solely from the parity products at  $\Gamma$  and *X*,  $(-1)^{\nu_0} = \delta_\Gamma \delta_X$  for our choice of origin. The 5*f* band with nontrivial parity switching leads to a strong topological state  $\nu_0=1$ . The other indices are all identical,  $\nu_1=\nu_2=\nu_3=1$ , determined from  $(-1)^{\nu_1} = \delta_X \delta_R \delta_S \delta_T$ . In a smaller *U* range that includes *U*=0 eV, the non-doped system now has a genuine insulating band gap where exactly the same 5*f* band provides  $\nu_0=1$ . The topological 5*f* band in focus is predominantly comprised of  $y(5y^2 - 3r^2)$  orbitals on each of the two *U* atoms forming a rung. At the  $\Gamma$  point, the wavefunction has opposite sign on these two atoms, and hence has positive parity; as sketched in Fig. 1(e), however, at the *X* point the wavefunction has the same sign on the two rung atoms and is therefore odd parity. Common to both *k* points is the U(1)-U(2) bond that connects different lattice points (different rungs). For the *U* used here (1.2 eV), this topological band gives rise to a Fermi surface that is centered on the *X*-point, in agreement with the Fermi pocket observed experimentally [26, 27]. More details of band structure analysis including the *U* dependency are found in Supplemental Material.

*Minimal Hamiltonian:* The topological band and the ferromagnetic rung interaction found by DFT [23] indicates that the sublattice degree of freedom due to the U atoms on a rung plays an important role in the low-energy physics. Surprisingly, this degree of freedom has not been explicitly considered previously in understanding the superconducting state in UTe<sub>2</sub>, nor in the related materials UGe<sub>2</sub>, URhGe, and UCoGe where a similar U sublattice structure appears [21]. Here we consider the role of this sublattice degree of freedom through the construction of a minimal model. In particular, the U atoms sit on sites of  $C_{2v}$  symmetry, for which only a single spinor symmetry representation exists. A minimal model therefore includes a single spinor pair centered on each of the sublattices. While these spinors share the same symmetry properties as usual spin-1/2 fermions under  $C_{2v}$  symmetry, DFT reveals they are generally a linear combination of *j* = 5/2 states. This model only includes two bands. However, we note ARPES measurements have observed only one Fermi pocket associated with the U 5*f* electrons [27], which are responsible for the superconducting state, suggesting this model is a reasonable description. The most general noninteracting Hamiltonian including all symmetry-allowed terms with sublattice and spin degrees of freedom is

$$H_N = \epsilon_0(k) - \mu + f_{A_g}(k)\tau_x + f_z(k)\tau_y + f_y(k)\sigma_x\tau_z + f_x(k)\sigma_y\tau_z + f_{A_u}(k)\sigma_z\tau_z \quad (1)$$

where the functions  $f_i(k)$  carry the symmetry properties

given by the label  $i$ , in particular  $f_{A_g}(k) \sim \text{constant}$ ,  $f_z(k) \sim k_z$ ,  $f_y(k) \sim k_y$ ,  $f_x(k) \sim k_x$ , and  $f_{A_u}(k) \sim k_x k_y k_z$ . Here the Pauli matrices  $\sigma_i$  describe the spin degrees of freedom and the Pauli matrices  $\tau_i$  describe the rung degrees of freedom. While our analysis below does not depend upon the detailed form of the  $f_i(k)$ , for the  $y(5y^2 - 3r^2)$  orbitals discussed above we obtain the following tight-binding theory

$$\begin{aligned}
\epsilon_0(k) &= t_1 \cos(k_x) + t_2 \cos(k_y) \\
f_{A_g}(k) &= m_0 + t_3 \cos(k_x/2) \cos(k_y/2) \cos(k_z/2) \\
f_z(k) &= t_z \sin(k_z/2) \cos(k_x/2) \cos(k_y/2) \\
f_y(k) &= t_y \sin(k_y) \\
f_x(k) &= t_x \sin(k_x) \\
f_{A_u}(k) &= t_u \sin(k_x/2) \sin(k_y/2) \sin(k_z/2). \quad (2)
\end{aligned}$$

Note that to replicate the nontrivial parity switching predicted above, the magnitude of the *inter-rung* U(1)-U(2) hopping  $t_3$  [see Fig. 1(e)] needs to exceed the *intra-rung* hopping  $m_0$ . Fitting to the DFT band near the Fermi surface gives  $(\mu, t_1, t_2, m_0, t_3, t_z, t_x, t_y, t_u) = (0.129, -0.0892, 0.0678, -0.062, 0.0742, -0.0742, 0.006, 0.008, 0.01)$ . This fit yields the Fermi surface shown in Fig 3.

*Magnetic interactions:* DFT calculations have found that the dominant magnetic interaction is a ferromagnetic interaction between the rung sublattice U atoms [23]. Note that this local ferromagnetic interaction does not imply a global ferromagnetic state, but only that these two U atoms have the same spin-orientation. Indeed, DFT finds ferromagnetic and anti-ferromagnetic ground states consistent with this local configuration [23], which may account for the two magnetically-ordered states observed experimentally [16]. This interaction is given by

$$H_{int} = - \sum_i (J_x S_{i,1}^x S_{i,2}^x + J_y S_{i,1}^y S_{i,2}^y + J_z S_{i,1}^z S_{i,2}^z) \quad (3)$$

where 1, 2 labels the two U atoms on the rung, and  $i$  labels a lattice point; the ferromagnetic interactions  $J_\mu > 0$  are in general unequal due to the orthorhombic structure. Treating this as an effective coupling for superconductivity, we find this gives rise to three possible pairing states as listed in Table I. Due to the inter-sublattice nature of the magnetic interactions, the gap functions are necessarily proportional to a non-trivial  $\tau_y$  sublattice operator and take the form  $\Delta_i \tau_y \sigma_i$  which describes a local, inter-sublattice, spin-triplet pairing function. While the interactions reveal the role of magnetic anisotropy on pairing interaction, we will now set  $J_x = J_y = J_z$  to examine the effect of  $H_N$  on these pairing states.

*Role of  $H_N$ :* Naively, the stable pairing state is determined by the largest interaction parameter listed in Table I. However, due to the spin-sublattice coupling in our model,  $H_N$  also influences the relative stability of the pairing states. The effect of the distinct terms in  $H_N$  on

TABLE I. Pairing gap functions due to ferromagnetic interactions between rung sublattice degrees of freedom. The first column gives the local gap function and the last column gives the corresponding  $\vec{d}(k)$  in the band basis when the spin-orbit coupling terms are vanishing ( $f_x = f_y = f_{A_u} = 0$ ).

Gap	Irrep	Interaction	Momentum dependence
$\Delta_z \tau_y \sigma_z$	$A_u$	$J_x + J_y - J_z$	$\frac{f_z(k)}{\sqrt{f_{A_g}^2(k) + f_z^2(k)}} \hat{z}$
$\Delta_x \tau_y \sigma_x$	$B_{2u}$	$-J_x + J_y + J_z$	$\frac{f_x(k)}{\sqrt{f_{A_g}^2(k) + f_x^2(k)}} \hat{x}$
$\Delta_y \tau_y \sigma_y$	$B_{3u}$	$J_x - J_y + J_z$	$\frac{f_y(k)}{\sqrt{f_{A_g}^2(k) + f_y^2(k)}} \hat{y}$

the transition temperature  $T_{c,i}$  of the state  $\Delta_i \tau_y \sigma_i$  can be quantified without fully specifying the functions  $f_j(k)$  using the concept of superconducting fitness [30, 31]: specifically, if the matrix  $\sigma_i \tau_j$  anticommutes with the gap function  $\Delta_i \tau_y \sigma_i$ , then the corresponding term in  $H_N$  will enhance  $T_{c,i}$ ; conversely,  $T_{c,i}$  is suppressed by this term if it commutes with the pairing potential [31]. This yields the result that the  $f_{A_g}$  term suppresses all the  $T_{c,i}$  and the  $f_z$  term enhances all the  $T_{c,i}$ . Consequently, if  $J_x = J_y = J_z$ , the spin-orbit coupling terms will dictate which  $T_{c,i}$  is highest. In particular, the largest  $T_{c,i}$  is given by the smallest of  $\langle f_{A_u}^2 \rangle$  ( $A_u$  stable),  $\langle f_x^2 \rangle$  ( $B_{3u}$  stable), or  $\langle f_y^2 \rangle$  ( $B_{2u}$  stable), where  $\langle \dots \rangle$  represents an average over the Fermi surface. The terms in the tight-binding expression will be altered by pressure, providing a potential explanation for the appearance of different superconducting states.

$H_N$  also dictates the form of the pseudospin triplet  $\vec{d}$ -vector on the Fermi surface. We do not give the details here but point out that generically, all three pseudospin components  $\hat{x}, \hat{y}, \hat{z}$  appear for each gap function. As we argue below, there is one limit that can be motivated by experimental results. In particular, when the momentum-dependent spin-orbit coupling terms are small, that is  $f_x^2, f_y^2, f_{A_u}^2 \ll f_z^2$  then the orientation of the spin-triplet  $\vec{d}$  vectors is set by the spin part of the gap function in Table I. In this case Table I provides an approximately correct description of  $\vec{d}$  (except near  $k_z = 0, 2\pi$ ); in the following this is called the weak spin-orbit coupling limit.

*Relationship to experiment:* At ambient pressure, two superconducting transitions in zero field and a polar Kerr effect that can be trained by a  $c$ -axis magnetic field has been observed [15]. The latter result implies a  $B_{3u} + iB_{2u}$  or a  $A_u + iB_{1u}$  pairing below the second transition [15]. In the context of our theory, the only possibility is the  $B_{3u} + iB_{2u}$  state. Such a broken-time reversal symmetry state can be stabilized by ferromagnetic fluctuations [15, 32, 33]. Assuming an isotropic rung ex-

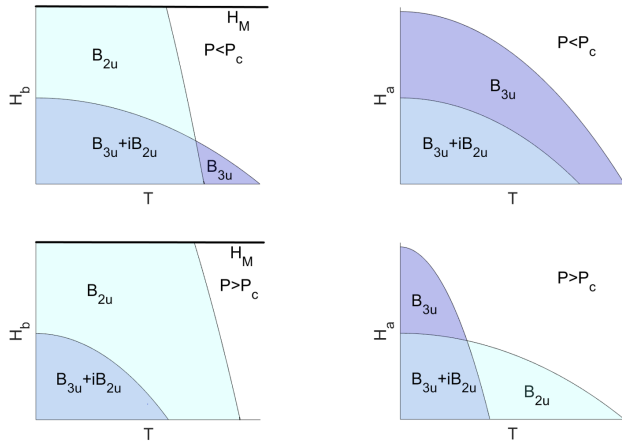


FIG. 2. Qualitative temperature-field phase diagrams for fields along the  $\hat{a}$  and  $\hat{b}$  directions. The top two phase diagrams correspond to  $P < 0.2$  GPa and the bottom two to  $P > 0.2$  GPa.  $H_M$  corresponds to an observed metamagnetic transition.

change, this situation arises in our model by requiring that  $\langle f_x^2 \rangle < \langle f_y^2 \rangle < \langle f_{A_u}^2 \rangle$ .

We note that additional consistency with experiment arises if we assume we are in the weak spin-orbit coupling limit. In particular, this limit naturally explains why thermal conductivity exhibits nodal behavior that is similar along both the  $\hat{a}$  and  $\hat{b}$  directions [25]: When  $f_x = f_y = f_{A_u} = 0$ , all the gap functions have accidental line nodes when  $k_z = 0$ , yielding nodal thermal conductivity behavior along both  $\hat{a}$  and  $\hat{b}$ . These accidental line nodes will be lifted when the spin-orbit coupling terms are non-zero, but if they are small we expect a local gap minimum near  $k_z = 0, 2\pi$  which can mimic nodes in thermal conductivity.

In addition, the weak spin-orbit coupling limit is consistent with the field dependence of the phase diagram for fields along the  $\hat{a}$  and  $\hat{b}$  as a function of pressure [14, 16, 34, 35]. In particular, in this limit the  $B_{3u}$  gap is primarily along  $\hat{b}$  and the  $B_{2u}$  gap is primarily along  $\hat{a}$ . This implies that the  $B_{3u}$  ( $B_{2u}$ ) gap will experience paramagnetic limiting for a field along  $\hat{b}$  ( $\hat{a}$ ) and not for the fields along  $\hat{a}$  ( $\hat{b}$ ). It has been observed that the two superconducting transitions cross at a critical pressure  $P_c \approx 0.2$  GPa [16]. In our model such a crossing should then be correlated with a switch in the upper critical field behavior for the field along the  $\hat{a}$  and  $\hat{b}$  directions, as shown in Fig. 2. This is indeed what is observed [1, 34, 35].

*Weyl Nodes:* Here we examine more carefully the nodal structure of a  $B_{3u} + iB_{2u}$  pairing state. Using the tight-binding theory given above, we find that Weyl nodes generically exist. These nodes are topologically protected but do not sit at positions of high symmetry. The po-

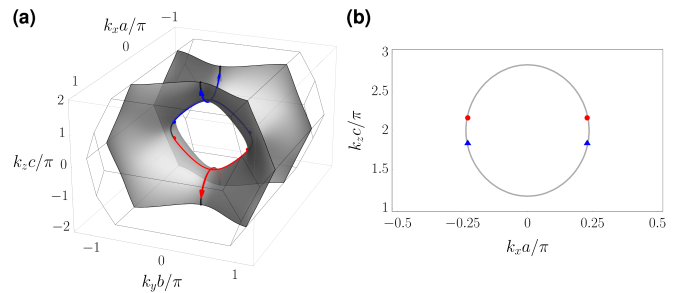


FIG. 3. (a) Evolution of Weyl nodes of  $B_{3u} + iB_{2u}$  pairing states by decreasing the relative amplitude of the  $B_{2u}$  gap pairing to the  $B_{3u}$  gap pairing. The gap amplitudes are chosen to be  $(\Delta_x, \Delta_y) = \Delta_0(\cos \theta, \sin \theta)$  where  $\theta$  is a real parameter. The Fermi surface is obtained from the tight-binding model fitted to the two DFT+ $U$  bands with  $U=1.2$  eV. Red and blue lines indicate trajectories of the nodes with +1 and -1 Weyl charge as  $\theta$  is varied. There are four nodes in a Brillouin zone and they sit on either the  $k_x$ - $k_z$  or the  $k_y$ - $k_z$  plane. (b) Weyl points on a  $k_x$ - $k_z$  slice. Triangles (blue) and circles (red) indicate +1 and -1 Weyl charge. The circular line is a cut of the Fermi surface and centered at the  $X$ -point.

sition of these nodes are determined by the relative amplitudes of the  $B_{2u}$  and the  $B_{3u}$  order parameters. The evolution of these nodes is shown in Fig. 3. We have also computed the Weyl charge of these nodes. Generically, there exists four Weyl nodes, two of charge +1 and two of charge -1. These Weyl nodes imply the existence of surface Fermi arc states which provide an explanation for the chiral edges states seen with scanning tunneling microscopy [20].

*Polar Kerr Effect:* Our multiband theory for the superconductivity in UTe<sub>2</sub> generically gives rise to an imaginary anomalous Hall conductivity, which is expected to be proportional to the polar Kerr signal. By a sum rule [36] we have that the integrated imaginary anomalous Hall conductivity is given by  $\int_{-\infty}^{\infty} \omega \sigma_H(\omega) d\omega = -i\pi e^2 \langle [\partial_{k_x} H_N, \partial_{k_y} H_N] \rangle$ . The full expansion of the commutator is very complicated and will be analyzed elsewhere, but we note that the contribution  $(\partial_{k_x} f_y \partial_{k_y} f_x - \partial_{k_x} f_x \partial_{k_y} f_y) \sigma_z \tau_0$  is directly proportional to the so-called time-reversal-odd bilinear of the  $B_{3u} + iB_{2u}$  pairing state [37, 38]. This implies that expectation value of the commutator is nonzero, ensuring the existence of the anomalous Hall conductivity and hence the polar Kerr signal. The presence of two bands due to the sublattice degree of freedom is critical to this argument; in a single-band model, the commutator is vanishing, and a polar Kerr effect does not appear in the clean limit [39].

From DFT+ $U$  calculations, we have identified a topological band near the chemical potential in UTe<sub>2</sub> that stems from U  $5f$  electrons. This result, together with the importance of rung ferromagnetic interactions, suggests that U atom rung degrees of freedom play an impor-

tant role in superconducting  $\text{UTe}_2$ . We have developed a model that includes these degrees of freedom and captures the topological bands. In addition, we show that including the ferromagnetic rung interactions allows a  $B_{3u} + iB_{2u}$  pairing state, accounting for Polar Kerr measurements and yielding Weyl points, providing a promising model with which to understand  $\text{UTe}_2$  in more detail. Similar U sublattice degrees of freedom exist in  $\text{UGe}_2$ ,  $\text{URhGe}$ , and  $\text{UCoGe}$ , suggesting a unifying motif for this class of materials.

We acknowledge useful discussions with Nick Butch, Yun Suk Eo, Ian Hayes, Aharon Kapitulnik, Johnpierre Paglione, Srinivas Raghu, and Di Wei. This work was supported by the U.S. Department of Energy, Office of Basic Energy Sciences, Division of Materials Sciences and Engineering under Award DE-SC0017632. P.M.R.B. was supported by the Marsden Fund Council from Government funding, managed by Royal Society Te Apārangi.

- 
- [1] S. Ran, C. Eckberg, Q.-P. Ding, Y. Furukawa, T. Metz, S. R. Saha, I.-L. Liu, M. Zic, H. Kim, J. Paglione, and N. P. Butch, *Science* **365**, 684 (2019).
- [2] D. Aoki, A. Nakamura, F. Honda, D. Li, Y. Homma, Y. Shimizu, Y. J. Sato, G. Knebel, J.-P. Brison, A. Pourret, D. Braithwaite, G. Lapertot, Q. Niu, M. Valika, H. Harima, and J. Flouquet, *Journal of the Physical Society of Japan* **88**, 043702 (2019), <https://doi.org/10.7566/JPSJ.88.043702>.
- [3] W. Knafo, M. Valika, D. Braithwaite, G. Lapertot, G. Knebel, A. Pourret, J.-P. Brison, J. Flouquet, and D. Aoki, *Journal of the Physical Society of Japan* **88**, 063705 (2019), <https://doi.org/10.7566/JPSJ.88.063705>.
- [4] A. Miyake, Y. Shimizu, Y. J. Sato, D. Li, A. Nakamura, Y. Homma, F. Honda, J. Flouquet, M. Tokunaga, and D. Aoki, *Journal of the Physical Society of Japan* **88**, 063706 (2019), <https://doi.org/10.7566/JPSJ.88.063706>.
- [5] S. Imajo, Y. Kohama, A. Miyake, C. Dong, M. Tokunaga, J. Flouquet, K. Kindo, and D. Aoki, *Journal of the Physical Society of Japan* **88**, 083705 (2019), <https://doi.org/10.7566/JPSJ.88.083705>.
- [6] V. P. Mineev, *JETP Letters* (2020), 10.1134/s0021364020120036.
- [7] S. Ran, H. Kim, I.-L. Liu, S. R. Saha, I. Hayes, T. Metz, Y. S. Eo, J. Paglione, and N. P. Butch, *Phys. Rev. B* **101**, 140503 (2020).
- [8] G. Knebel, M. Kimata, M. Valika, F. Honda, D. Li, D. Braithwaite, G. Lapertot, W. Knafo, A. Pourret, Y. J. Sato, Y. Shimizu, T. Kihara, J.-P. Brison, J. Flouquet, and D. Aoki, *Journal of the Physical Society of Japan* **89**, 053707 (2020), <https://doi.org/10.7566/JPSJ.89.053707>.
- [9] Q. Niu, G. Knebel, D. Braithwaite, D. Aoki, G. Lapertot, G. Seyfarth, J.-P. Brison, J. Flouquet, and A. Pourret, *Phys. Rev. Lett.* **124**, 086601 (2020).
- [10] S. Ran, I.-L. Liu, Y. S. Eo, D. J. Campbell, P. M. Neves, W. T. Fuhrman, S. R. Saha, C. Eckberg, H. Kim, D. Graf, F. Balakirev, J. Singleton, J. Paglione, and N. P. Butch, *Nature Physics* **15**, 1250 (2019).
- [11] Y. Tokunaga, H. Sakai, S. Kambe, T. Hattori, N. Higa, G. Nakamine, S. Kitagawa, K. Ishida, A. Nakamura, Y. Shimizu, Y. Homma, D. Li, F. Honda, and D. Aoki, *Journal of the Physical Society of Japan* **88**, 073701 (2019), <https://doi.org/10.7566/JPSJ.88.073701>.
- [12] S. Sundar, S. Gheidi, K. Akintola, A. M. Cote, S. R. Dunsiger, S. Ran, N. P. Butch, S. R. Saha, J. Paglione, and J. E. Sonier, *Phys. Rev. B* **100**, 140502 (2019).
- [13] G. Nakamine, S. Kitagawa, K. Ishida, Y. Tokunaga, H. Sakai, S. Kambe, A. Nakamura, Y. Shimizu, Y. Homma, D. Li, F. Honda, and D. Aoki, *Jour. Phys. Soc. Jpn.* **88**, 113703 (2019).
- [14] D. Braithwaite, M. Valiska, G. Knebel, G. Lapertot, J.-P. Brison, A. Pourret, M. E. Zhitomirsky, J. Flouquet, F. Honda, and D. Aoki, *Communications Physics* **2**, 147 (2019).
- [15] I. M. Hayes, D. S. Wei, T. Metz, J. Zhang, Y. S. Eo, S. Ran, S. R. Saha, J. Collini, N. P. Butch, D. F. Agterberg, A. Kapitulnik, and J. Paglione, (2020), arXiv:2002.02539 [cond-mat.str-el].
- [16] S. M. Thomas, F. B. Santos, M. H. Christensen, T. Asaba, F. Ronning, J. D. Thompson, E. D. Bauer, R. M. Fernandes, G. Fabbris, and P. F. S. Rosa, “Evidence for a pressure-induced antiferromagnetic quantum point in intermediate valence  $\text{UTe}_2$ ,” (2020), arXiv:2005.01659 [cond-mat.str-el].
- [17] K. Machida, *Journal of the Physical Society of Japan* **89**, 033702 (2020), <https://doi.org/10.7566/JPSJ.89.033702>.
- [18] S. Kittaka, Y. Shimizu, T. Sakakibara, A. Nakamura, D. Li, Y. Homma, F. Honda, D. Aoki, and K. Machida, *Phys. Rev. Research* **2**, 032014 (2020).
- [19] S. Bae, H. Kim, S. Ran, Y. S. Eo, I.-L. Liu, W. Fuhrman, J. Paglione, N. P. Butch, and S. Anlage, “Anomalous normal fluid response in a chiral superconductor,” (2019), arXiv:1909.09032 [cond-mat.supr-con].
- [20] L. Jiao, S. Howard, S. Ran, Z. Wang, J. O. Rodriguez, M. Sigrist, Z. Wang, N. P. Butch, and V. Madhavan, *Nature* **579**, 523 (2020).
- [21] D. Aoki, K. Ishida, and J. Flouquet, *J. Phys. Soc. Jpn.* **88**, 022001 (2019).
- [22] A. B. Shick and W. E. Pickett, *Phys. Rev. B* **100**, 134502 (2019).
- [23] Y. Xu, Y. Sheng, and Y.-F. Yang, *Phys. Rev. Lett.* **123**, 217002 (2019).
- [24] J. Ishizuka, S. Sumita, A. Daido, and Y. Yanase, *Phys. Rev. Lett.* **123**, 217001 (2019).
- [25] T. Metz, S. Bae, S. Ran, I.-L. Liu, Y. S. Eo, W. T. Fuhrman, D. F. Agterberg, S. Anlage, N. P. Butch, and J. Paglione, *Phys. Rev. B* **100**, 220504 (2019).
- [26] S.-i. Fujimori, I. Kawasaki, Y. Takeda, H. Yamagami, A. Nakamura, Y. Homma, and D. Aoki, *Journal of the Physical Society of Japan* **88**, 103701 (2019), <https://doi.org/10.7566/JPSJ.88.103701>.
- [27] L. Miao, S. Liu, Y. Xu, E. C. Kotta, C.-J. Kang, S. Ran, J. Paglione, G. Kotliar, N. P. Butch, J. D. Denlinger, and L. A. Wray, *Phys. Rev. Lett.* **124**, 076401 (2020).
- [28] M. Weinert, G. Schneider, R. Podlucky, and J. Redinger, *J. Phys. Condens. Matter* **21**, 084201 (2009).
- [29] L. Fu and C. L. Kane, *Phys. Rev. B* **76**, 045302 (2007).
- [30] A. Ramires and M. Sigrist, *Phys. Rev. B* **94**, 104501 (2016).
- [31] A. Ramires, D. F. Agterberg, and M. Sigrist, *Phys. Rev. B* **98**, 024501 (2018).
- [32] V. G. Yarzhemsky and E. A. Teplyakov, “Time-reversal symmetry and the structure of superconducting order

- Parameter of nearly ferromagnetic spin-triplet superconductor  $UTe_2$ ,” (2020), arXiv:2001.02963 [cond-mat.supr-con].
- [33] A. H. Nevidomskyy, “Stability of a nonunitary triplet pairing on the border of magnetism in  $UTe_2$ ,” (2020), arXiv:2001.02699 [cond-mat.supr-con].
- [34] D. Aoki, F. Honda, G. Knebel, D. Braithwaite, A. Nakamura, D. Li, Y. Homma, Y. Shimizu, Y. J. Sato, J.-P. Brison, and J. Flouquet, *Journal of the Physical Society of Japan* **89**, 053705 (2020), <https://doi.org/10.7566/JPSJ.89.053705>.
- [35] W.-C. Lin, D. J. Campbell, S. Ran, I.-L. Liu, H. Kim, A. H. Nevidomskyy, D. Graf, N. P. Butch, and J. Paglione, “Tuning magnetic confinement of spin-triplet superconductivity,” (2020), arXiv:2002.12885 [cond-mat.supr-con].
- [36] E. Lange and G. Kotliar, *Phys. Rev. Lett.* **82**, 1317 (1999).
- [37] P. M. R. Brydon, D. F. Agterberg, H. Menke, and C. Timm, *Phys. Rev. B* **98**, 224509 (2018).
- [38] P. M. R. Brydon, D. S. L. Abergel, D. F. Agterberg, and V. M. Yakovenko, *Phys. Rev. X* **9**, 031025 (2019).
- [39] E. Taylor and C. Kallin, *Phys. Rev. Lett.* **108**, 157001 (2012).